Nuclear Instruments and Methods in Physics Research B 268 (2010) 341–345

Contents lists available at ScienceDirect

Nuclear Instruments and Methods in Physics Research B

journal homepage: www.elsevier.com/locate/nimb

Structural distortion of biogenic aragonite in strongly textured mollusc shell layers

D. Chateigner [a,*], S. Ouhenia [a,b], C. Krauss [a], M. Belkhir [b], M. Morales [c]

[a] CRISMAT-ENSICAEN, Université de Caen Basse-Normandie, 6 Bd. M. Juin, 14050 Caen, France
[b] Lab. De Physique, Faculté des Sciences Exactes, Bejaia 06000, Algeria
[c] CIMAP-ENSICAEN, Université de Caen Basse-Normandie, 6 Bd. M. Juin, 14050 Caen, France

ARTICLE INFO

Article history:
Received 30 May 2009
Received in revised form 9 July 2009
Available online 17 July 2009

Keywords:
Texture
Mollusc shell
Pinctada
Charonia
Haliotis
Nacre

ABSTRACT

The stabilisation of strong textures in mollusc shells has for long been a strong drawback towards precise structural determinations of these natural biocomposites. We demonstrate here on several crossed lamellar and nacre layers from two gastropods (*Charonia lampas lampas* and *Haliotis tuberculata tuberculata*) and one bivalve (*Pinctada maxima*), that on real specimens (without grinding or specific preparation), the textural information can be used efficiently for precise structural determination of the biogenic aragonite. This is done through the combination of orientation distribution function and cyclic Rietveld refinements on several hundreds to thousands of diffractions diagrams.

1. Introduction

Mollusc shells are fascinating organic-mineral biocomposites with high mechanical performances. With only 1–5 wt% of organic material [1,2], a nanometer-sized growth-control is achieved which increases the shell toughness and mechanical properties considerably compared to the non-biogenic mineral. For instance, nacre hardness from the red abalone *Haliotis rufescens* is 3000× larger than the one of the mineral [3–5]. Both hardness and low crack propagation in nacre are attributed to strong structural bounds between organic macromolecules and inorganic crystals [6,7]. Mollusc shells are mainly made of calcite and aragonite crystalline polymorphs. The major part of organic materials is intercrystalline, and in a minor way intracrystalline. Recently, using high resolution synchrotron radiation, Pokroy et al. [8,9] showed that the biogenic unit-cells are deformed anisotropically compared to the non-biogenic crystals. The distortions observed by these authors are due to intracrystalline organic molecules. This corresponds to a stabilisation of the metastable biogenic aragonite via intermediate aplanarity of the carbonate groups, between a perfect plane for calcite and non-biogenic aragonite [10]. However, all the previous X-ray and neutron studies were done on powderised samples, with the samples being composed of several shell layers and eventually several phases.

In this work we made use of the so-called "Combined Analysis" [11] to determine simultaneously the structure (unit-cell distortions and atomic positions) and the preferred orientations (texture) of constituting aragonite crystallites of several shell layers. We chose samples of the crossed lamellar layers of the gastropod *Charonia lampas lampas*, the inner columnar nacre from *Haliotis tuberculata tuberculata* and the inner nacre layer of *Pinctada maxima* in order to compare cell distortions and structural modifications between these widespread layer types. This approach was chosen because it allows working on real samples, without grinding operation or specific preparation.

2. Samples and experiments

2.1. Mollusc shell species

C. lampas lampas (Linnaeus 1758) is a large carnivorous gastropod from the Ranellidae (to which tritons and trumpets belong) [12,13], Caenogastropoda. We collected a 15 cm deceased animal from the Bejaia county, North-West Algeria. The inorganic part of the shell is only composed of three different crossed lamellar aragonitic layers as revealed by SEM [14]. The bivalve *P. maxima* (Röding 1798) collected in the French Polynesia offers a large brick-wall (sheet) nacre layer (ISN) in its inner part. The gastropod *H. tuberculata tuberculata* (Linnaeus 1758) was collected in the North-Cotentin coastal range, France. The shell is made of an inner nacre layer and an outer calcitic layer. We analysed the Inner Columnar Nacre (ICN) layer.

X-ray diffraction combined analysis was done on specimens that were as flat as possible from the shell dorsum. The sample

* Corresponding author.
E-mail address: daniel.chateigner@ensicaen.fr (D. Chateigner).

0168-583X/$ - see front matter © 2009 Elsevier B.V. All rights reserved.
doi:10.1016/j.nimb.2009.07.007

reference frame was chosen as in previous studies using the main shell directions (*G*,*N*,*M*) [15]:

- the growth direction, *G*, normal to the shell margin is the vertical axis of our pole figures;
- the plane tangent to the shell at the beam location has its normal, *N*, in the center of the pole figures;
- the third axis, *M*, is the margin direction, often corresponding to growth lines on the shell surface, and is horizontal on the pole figures.

Each layer was measured successively, from the outer to the inner, by removing capping layers using HCl, inward.

Using the terminology of Carter and Clark [16], the shell of *C. lampas lampas* is constituted by three crossed lamellar layers, outer comarginal (OCL), radial (IRCL) and comarginal (ICCL) from top to bottom, though the top layer is not a regular one [14]. In the case of *P. maxima* and *H. haliotis*, we analysed the inner nacre layers, of sheet (ISN) and columnar (ICN) natures, respectively.

2.2. Combined texture–structure X-ray analysis

Diffraction measurements were done on a 4-circle diffractometer equipped with a curved position sensitive detector (CPS 120, Inel) using copper monochromatic Kα radiation [17]. The use of a 1D detector covering an enough large 2θ range is essential for a reasonable total acquisition time of the necessary diagrams. We used a $5^\circ \times 5^\circ$ grid in tilt (χ) and azimuth (ϕ) and covered the pole figures up to 60° in χ, resulting in 936 diagrams per each layer, for *C. lampas* and *H. tuberculata*, while for *P. maxima* a $2.5^\circ \times 2.5^\circ$ grid was used, resulting in 3744 diagrams. Such an acquisition gives access to the possibility of refining texture, cell parameters, atomic positions, etc. Pole figures are normalised in distribution density units (or m.r.d. for multiple of a random distribution), a unit depending only on orientation. In such units, a specimen without any preferred orientation exhibits 1 m.r.d. homogeneous levels on all pole figures, while a textured specimen shows minima and maxima of the densities. Instrumental resolution was calibrated using the NIST LaB_6 (SRM 660b) standard. Data treatment is done through the "Combined Analysis" formalism [11] implemented in the MAUD software [18]. The Orientation Distributions (ODs) of crystallites were refined within the E-WIMV formalism [19], and intensity extractions were done using the Le Bail [20] approach. No residual stress could be observed in the layers.

3. Results and discussion

3.1. Textures and cell distortions

3.1.1. Crossed lamellar layers of C. lampas lampas

Combined analysis refinements on the three layers converged to solutions corresponding to good reliability factors and maximum GoF values of 3.05 (Table 1). Reliability factors might appear large compared to those reported in the literature. However one has to bear in mind that such factors depend on the number of measured points, which in our case is around 1.8×10^6, with 1900 points/diagram and 936 diagrams. The OD reliability factors compare well with the literature for similar texture strengths [21]. The refinement quality can be visualised by comparing experimental and recalculated diagrams for selected diagrams and for the whole experimental set (Fig. 1).

For all layers, the minimum OD values are 0, indicating that all crystallites are oriented within the texture components. In *Charonia*, from the outer layer inward, the texture index increases, indicating a larger crystallite organisation closer to the animal, as has been observed already for many species [15]. The maximum OD value observed for the intermediate layer is small because of the existence of two texture components in this layer, each component being strongly oriented. The outer OCCL layer exhibits a global texture strength $F^2 = 42.6$ m.r.d.^{2}, which is among the moderate strengths in the gastropod shells that have been measured already [15], and is mainly due to the fibre character of the texture (Fig. 2(a)). The {0 0 2} pole figure shows a maximum distribution density in its center around 43 m.r.d., which is among the largest values for crossed lamellar layers [15], and indicates that all the

Table 1
Combined analysis results for the three crossed lamellar layers of *Charonia lampas lampas*. Standard deviations on the last digit are given in the parentheses. GoF: Goodness of Fit. Cell parameters references for the non-biogenic aragonite are: $a = 4.9623(3)$ Å, $b = 7.968(1)$ Å, $c = 5.7439(3)$ Å (ICDD file No. 41-1475).

Shell		*Charonia lampas lampas*			*Pinctada maxima*	*Haliotis tuberculata tuberculata*
Layer		OCL	IRCL	ICCL	ISN	ICN
a (Å)		4.98563(7)	4.97538(4)	4.9813(1)	4.97071(4)	4.9480(2)
b (Å)		8.0103(1)	7.98848(8)	7.9679(1)	7.96629(6)	7.9427(6)
c (Å)		5.74626(3)	5.74961(2)	5.76261(5)	5.74804(2)	5.7443(6)
$\Delta a/a$		0.0047	0.0026	0.0038	0.0017	−0.0029
$\Delta b/b$		0.0053	0.0026	0.0000	−0.0002	−0.0032
$\Delta c/c$		0.0004	0.0010	0.0033	0.0007	0.0007
$\Delta V/V$ (10^{-2})		1.05	0.62	0.71	0.22	−0.6
OD maximum (m.r.d.)		299	196	2816	3070	1500
OD minimum (m.r.d.)		0	0	0	0	0
Texture index (m.r.d.^{2})		42.6	47	721	1113	211
OD reliability	R_w(%)	14.3	11.2	32.5	21.9	36.1
Rietveld reliability	GoF	1.72	1.72	3.05	3.34	9.9
	R_w(%)	29.2	28.0	57.3	34.86	42.9
	R_{exp}(%)	22.2	21.3	32.8	19.07	13.6
Ca	y	0.41418(5)	0.414071(4)	0.41276(9)	0.41479(3)	0.4148(9)
	z	0.75939(3)	0.76057(2)	0.75818(8)	0.75939(2)	0.7582(1)
C	y	0.7628(2)	0.76341(2)	0.7356(4)	0.7676(1)	0.7850(4)
	z	−0.0920(1)	−0.08702(9)	−0.0833(2)	−0.0831(1)	−0.0886(1)
O1	y	0.9115(2)	0.9238(1)	0.8957(3)	0.9134(1)	0.9518(6)
	z	−0.09205(8)	−0.09456(6)	−0.1018(2)	−0.09255(7)	−0.1042(1)
O2	x	0.4768(1)	0.4754(1)	0.4864(3)	0.4678(1)	0.4583(9)
	y	0.6826(1)	0.68332(9)	0.6834(2)	0.68176(7)	0.6928(2)
	z	−0.08368(6)	−0.08473(5)	−0.0926(1)	−0.09060(4)	−0.0874(6)
ΔZ_{C-O1} (Å)		0.00029	0.04335	0.1066	0.054	0.0895

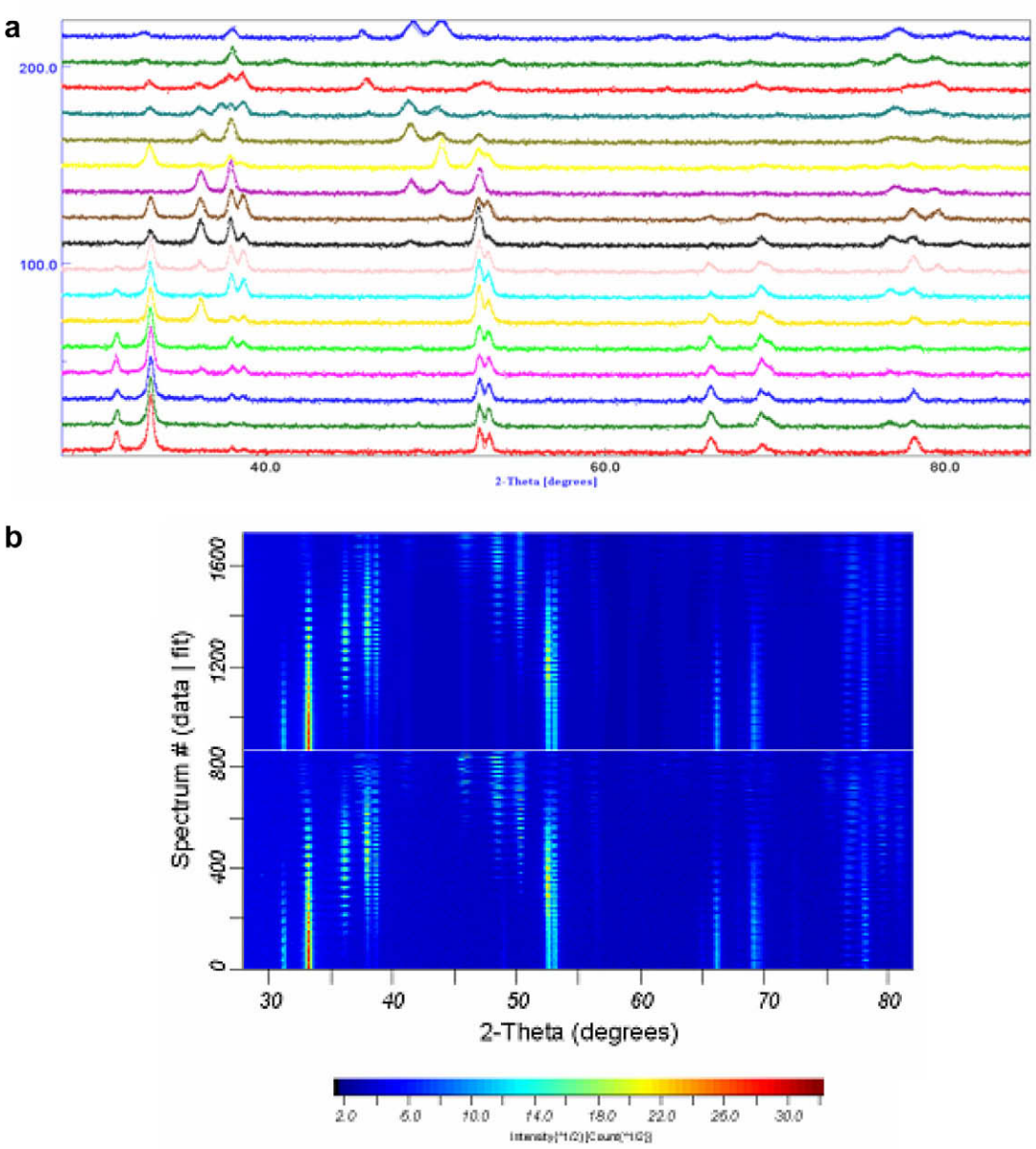

Fig. 1. Experimental and recalculated diagrams showing the typical refinement quality on our samples (here the IRC layer of *Charonia lampas lampas*) (a) For selected (χ,ϕ) sample orientations and (b) for all (χ,ϕ) orientations (the top diagrams are simulations, and the bottom diagrams are experiments).

crystallites tend to align their *c* axes along *N*, with a Half-Width at Half-Maximum of the density (HWHD) around 20°. The intermediate IRCL layer exhibits a texture strength of 47 m.r.d.^{2} and a maximum density for the {0 0 2} pole figure at 25.5 m.r.d. (Fig. 2(b)). The {0 0 2} pole figure shows two orientation components with *c* axes inclined and distributed around *N*, with 20° between the two components, in the (*G*,*N*) plane, each showing a FWHD of 10°. The {2 0 0} and {0 2 0} pole figures indicate a single {1 1 0} twin-like pattern [15], with the major component having ⟨1 1 0⟩ directions parallel to *M*, similar to *Patella tabularis* textures. The inner ICCL layer (Fig. 2(c)) exhibits the strongest texture for this shell with 720 m.r.d.^{2} of global strength and a {0 0 2} pole figure maximum of 102 m.r.d., which is among the strongest values observed in shells to date. Two texture components at 20° from *N*, with *c* axes in the (*M*,*N*) plane are observed. However four other 0 0 2 lower poles are present, as a sign of double twin-like pattern, as perhaps more evidently seen on the {0 2 0} pole figure showing six poles.

3.1.2. Nacre layers of P. maxima and H. tuberculata tuberculata

The inner sheet nacre layer of *P. Maxima* appears to be very much textured, with F^2 = 1247 m.r.d.^{2} due to both the strong alignment of the *c* axes along *N* (which is inclined due to a miscut of the shell in this case) and the alignment of *a* and *b* axes in the (*G*,*M*) plane, resulting in a double twin-like pattern. The refinement converges to a R_w of 21.95% and a GoF of 4.8. The texture strength results in a maximum density on the {0 0 2} pole figure of 208 m.r.d., which is about the largest observed up to now on mollusc shells. (Fig. 3(a)), in agreement with the results reported by Rousseau et al. [22]. Unit-cell distortions are also observed for this layer.

In the case of *H. tuberculata tuberculata*, the texture is fibre-like with a <0 0 1> fibre axis parallel to *N* (Fig. 3(b)), with a maximum density of 75 m.r.d. on the {0 0 2} pole figure, which is typical of a columnar nacre as for other *Haliotis* species that have been characterised already [15].

The refined cell parameters of all the layers exhibit cell distortions compared to non-biogenic aragonite. However, only the nacre

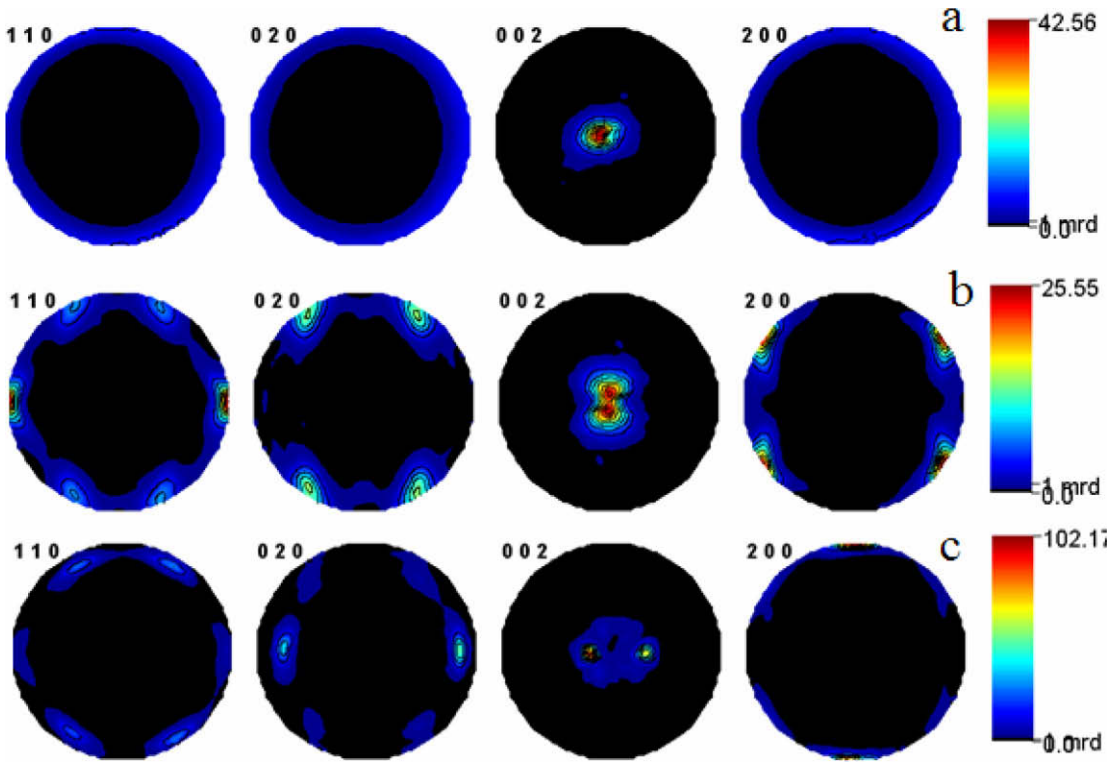

Fig. 2. {1 1 0}, {0 2 0}, {0 0 2} and {2 0 0} normalised pole figures of the (a) outer (b) intermediate and (c) inner layers of *Charonia lampas lampas*.

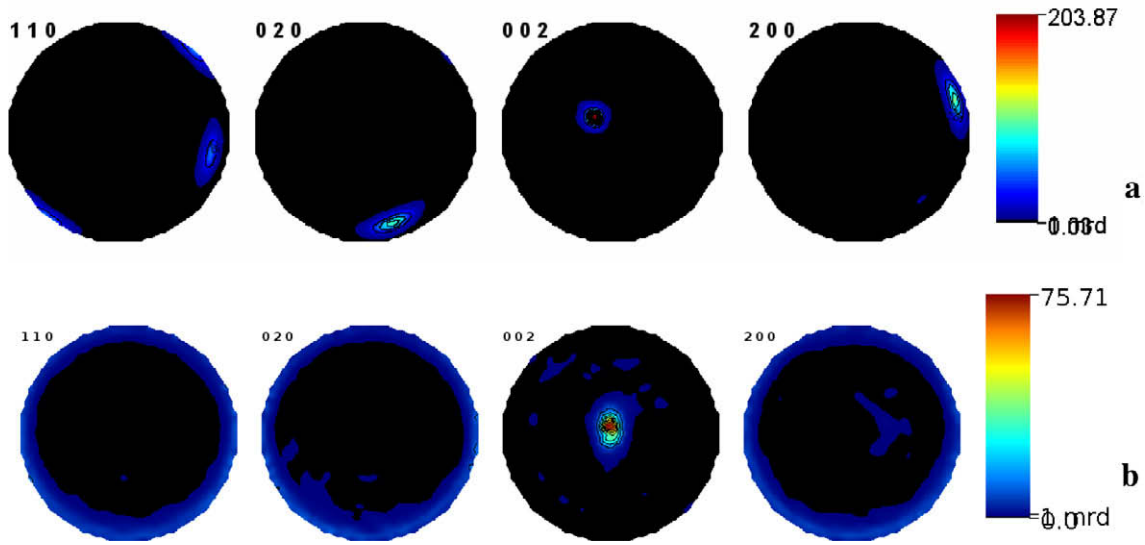

Fig. 3. {1 1 0}, {0 2 0}, {0 0 2} and {2 0 0} normalised pole figures of the (a) ISN layer of *Pinctada maxima* and (b) ICN layer of *Haliotis tuberculata tuberculata*.

layers show some cell parameter contraction, in the (*a*,*b*) plane of aragonite. The cell distortions are anisotropic and the relative volumic variations are variable among the layers of different shells as well as in the same shell. Biogenic distortions have been observed already [9] on powderised aragonitic mollusc shell layers. However the observed distortions were about three times smaller than our maximum distortion, mainly because of a specific preparation to remove intercrystalline molecules. Pokroy [10] attributed these distortions to the carbonate group aplanarity. In our case we measured real layers, not powderised nor bleached, and the distortions observed come from both intercrystalline and intracrystalline molecules. Even if intercrystalline molecules were associated to the calcium carbonate polymorph selection [23], and to the peculiar crystallites organisation in the shells, one cannot exclude an effect of the former on the cells distortion. Since a strong bonding exists between these molecules and the mineral to promote orientation, they are also probably largely responsible for the anisotropic character of the unit-cell distortion. This would explain why our cell distortions are larger than the ones observed in the case of solely intracrystalline molecules. Furthermore, grinding the layers for measurements could influence the distortion characterisation, on one hand because imposed stresses by intercrystalline molecules

could be partially removed, and on the other hand because texture removal could give rise to less observed anisotropy as was demonstrated on crystallite shape analysis [24].

All the textured layers show a unit-cell distortion anisotropy which is different from the one uniquely due to intracrystalline molecules. The most deformed cell parameters depend on the layer type. There is then a strong relationship between the way the unit-cells are deformed and the layer texture. For instance, all cell parameters are extended in the measured crossed lamellar layers, while the nacre layers exhibit compressed (*a*,*b*) planes and a rather elongated *c* axis. One should notice that no residual stress could be detected in the layers. All molecules are then intimate parts of new biocomposite crystals and not only intercalated entities deserving new stabilised states of known crystals. In the case of *C. lampas*, second order lamellaes are inclined with respect to the *c* axes of aragonite [14]. This gives rise to a global expansion of the unit-cells, while in nacres in which substructures of each nacre platelet are parallel to the plane of the platelets, the cell distortions appear more anisotropic. The cell distortion is clearly different between the two observed nacres. In the columnar nacre the (*a*,*b*) planes appear compressed along the two main directions while for sheet nacre a small compression is only observed along *b*, and an elongation along *a*, both remaining much smaller in magnitude than in the ICN layer of *H. tuberculata*. This anisotropy of the distortion in the (*a*,*b*) plane for ISN layers could be linked to the preferential etching by sodium hypochlorite, while absent in *H. tuberculata,* as observed by Mutvei and Dunca [25].

3.2. Structures

The refined atomic positions (Table 2) are also obtained within good standard deviations, even for C and O atoms. Thermal vibrations were fixed during the refinement, because of the lack of sensitivity on the latter in our diffraction range. One estimate of structural modifications for aragonite is the distance $\Delta Z_{C-O1} = (z_C - z_{O1})c$ between carbon and oxygen planes revealing aplanarity of the carbonate groups [9]. This distance goes from 0 Å for calcite to 0.057 Å for non-biogenic aragonite. In the crossed lamellar layers of *Charonia*, the latter increases from the outer layer to the inner layer, where it reaches 0.1 Å. The average value of ΔZ_{C-O1} on the three *Charonia* layers is 0.05 Å, i.e. the value for mineral aragonite. Hence, simple grinding of the three layers together would have biased the results, masking organic effects. Of course the average can differ for each layer type, and this is valid only for *Charonia*. In this species, carbonate aplanarity is larger in the inner layer, and then decreases in the intermediate layer, to practically vanish in the outer layer. On many mollusc shells a calcite layer is located outside, and such a quasi-zero aplanarity finally in the outer layer expresses, together with the loss in texture strength, the progressive control loss of organic matter farther from the animal. In the two analysed nacre layers, the ΔZ_{C-O1} values are intermediate compared to the ones of *Charonia*, but there is a clear tendency for a larger one in the columnar layer of *Haliotis*. In the latter the value is even 50% larger than that for non-biogenic aragonite, which corresponds to a larger stabilised energetic state. Such a larger internal energy is linked to the less compact microstructures of ICN compared to ISN layers, as observed using SEM by many authors, and to a lower crystallite organisation. It could explain why in natural conditions nacres from *Haliotis* dead shells are subjected to severe delamination, and usually are found in less intact shapes compared to other nacre type shells.

4. Conclusion

Combined analysis used for the characterisation of real layers from several shells offered precise determinations of crystallite preferred orientations, together with unit-cell distortions and structural modifications stabilised by organic macromolecules. Strong textures are observed in all the studied layers, involving angular relationships similar to single-crystal analyses that help the structural determinations within good resolutions, via ODF refinements.

Acknowledgement

The authors are indebted to the Conseil Régional Basse-Normandie, who financed part of the X-ray instrumental setup.

References

[1] P.E. Hare, P.H. Abelson, Year Book, Carnegie Inst. Washington, Vol. 65, 1965, p. 223.
[2] M.A. Cariolou, D. Morse, J. Comp. Phys. B 157 (1988) 717.
[3] J.D. Currey, Proc. Roy. Soc. Lond. B, Biol. Sci. 196 (1977) 443.
[4] A.P. Jackson, J.F.V. Vincent, R.M. Turner, J. Mat. Sci. 25 (1990) 3173.
[5] S. Kamat, X. Su, R. Ballarini, A.H. Heuer, Nature 405 (2000) 1036.
[6] B. Chen, X. Peng, J. Wang, S. Sun, Comp. Mat. Sci. 4 (2008) 201.
[7] B.L. Smith, T.E. Schaffer, M. Viani, J.B. Thompson, N.A. Frederick, J. Kind, A. Belcher, G.D. Stucky, D.E. Morse, P.K. Hansman, Nature 399 (1999) 761.
[8] B. Pokroy, J.P. Quintana, E.N. Caspi, A. Berner, E. Zolotoyabko, Nature Mat. 3 (2004) 900.
[9] B. Pokroy, A.N. Fitch, P.L. Lee, J.P. Quintana, E.N. Caspi, E. Zolotoyabko, J. Struc. Biol. 153 (2006) 145.
[10] B. Pokroy, J.S. Fieramosca, R.B. Von Dreele, A.N. Fitch, E.N. Caspi, E. Zolotoyabko, Chem. Mat. 19 (2007) 3244.
[11] D. Chateigner, in: D. Chateigner (Ed.) Combined Analysis: Structure–Texture–Microstructure–Phase–Stresses–Reflectivity Analysis by X-ray and Neutron Scattering, ISTE, 2009, 295p.
[12] A.G. Beu, Conchologists Am. Bull. 13 (1985) 55.
[13] A.G. Beu, New Zealand J. Zool. 13 (1987) 241.
[14] S. Ouhenia, D. Chateigner, M. Belkhir, E. Guilmeau, J. Struc. Biol. 163 (2008) 175.
[15] D. Chateigner, C. Hedegaard, H.-R. Wenk, J. Struc. Geol. 22 (2000) 1723.
[16] J.G. Carter, G.R. Clark II, in: D.J. Bottjer, C.S. Hickman, P.D. Ward, T.W. Broadhead (Eds.), Molluscs, Notes for a Short Course, Univ. Tennessee Dept. Geol. Sci. Stud. Geol., p. 50.
[17] M. Morales, D. Chateigner, L. Lutterotti, J. Ricote, Mat. Sci. For. 408–412 (2002) 1055.
[18] L. Lutterotti, S. Matthies, H.-R. Wenk, National Research Council of Canada, Ottawa, 1999, p. 1599.
[19] L. Lutterotti, D. Chateigner, S. Ferrari, J. Ricote, Thin Sol. Films 450 (2004) 34.
[20] A. Le Bail, Powder Diffract. 20 (2005) 316.
[21] D. Chateigner, J. Appl. Cryst. 38 (2005) 603.
[22] M. Rousseau, E. Lopez, P. Stempfle, M. Brendle, L. Franke, A. Guette, R. Naslain, X. Bourrat, Biomaterials 26 (2005) 6254.
[23] G. Falini, S. Albeck, S. Weiner, L. Addadi, Science 271 (1996) 67.
[24] M. Morales, Y. Leconte, R. Rizk, D. Chateigner, J. Appl. Phys. 97 (2005) 34307.
[25] H. Mutvei, E. Dunca, Paläont. Zeit. 82 (2008) 85.